In Situ-formed Fibrin Hydrogel Scaffold Loaded With Human Umbilical Cord Mesenchymal Stem Cells Promotes Skin Wound Healing

Lvzhong Hu
First Affiliated Hospital of Soochow University https://orcid.org/0000-0001-8026-664X
Jinhua Zhou
First Affiliated Hospital of Soochow University
Zhisong He
First Affiliated Hospital of Soochow University
Lin Zhang
First Affiliated Hospital of Soochow University
Fangzhou Du
Suzhou Institute of Biomedical Engineering and Technology
Mengting Nie
Suzhou Institute of Biomedical Engineering and Technology
Yao Zhou
First Affiliated Hospital of Soochow University
Hang Hao
Suzhou Institute of Biomedical Engineering and Technology
Lixing Zhang
Suzhou Institute of Biomedical Engineering and Technology
Shuang Yu
Suzhou Institute of Biomedical Engineering and Technology
Jinzhong Zhang
Suzhou Institute of Biomedical Engineering and Technology
Youguo Chen (chenyouguo@suda.edu.cn)
First Affiliated Hospital of Soochow University

Research

Keywords: Human umbilical cord mesenchymal stem cells, hydrogel, fibrin, skin wound healing

Posted Date: December 31st, 2020

DOI: https://doi.org/10.21203/rs.3.rs-136523/v1

Abstract

Background: Full-thickness skin wound healing remains a major challenge. Recently, human umbilical cord mesenchymal stem cells (hUC-MSCs) have exerted their brilliant potential to promote skin repair in clinical applications. However, low survival rate of hUC-MSCs after transplantation limits their therapeutic efficiency in treating full-thickness skin wound. The fibrin hydrogel is considered an ideal cell transplantation vectors owing to its three-dimensional mesh structure and low cytotoxicity. The objective of this study was to investigate the skin wound healing effect of fibrin hydrogel scaffold loaded with hUC-MSCs.

Methods: The cytotoxicity of the fibrin hydrogel was determined via cell counting kit-8 (CCK-8) assay. A total of 36 mice aged 8 weeks were randomly divided into four groups: control group (n = 9); hydrogel-alone group (n = 9); hUC-MSC-alone group (n = 9); and hydrogel-hUC-MSC combination group (n = 9). PBS, fibrin hydrogel, hUC-MSCs or fibrin hydrogel loaded with hUC-MSCs were injected into wounds, respectively. The wound of each mice was recorded with a digital camera to calculate the wound healing rate. On days 3, 7 and 14, serial sections of the wound and surrounding tissues were prepared. Hematoxylin and eosin staining, immunofluorescent staining for green fluorescent protein, keratin 10, and keratin 14 were performed. Meanwhile, the expressions of vascular endothelial growth factor A (VEGFA), vascular endothelial growth factor (VEGF), epidermal growth factor (EGF), and transforming growth factor-β1 (TGF-β1) were detected using RT-PCR.

Results: We found that the fibrin hydrogel owned three-dimensional mesh structure and low cytotoxicity, and could prolong the cell survival time around the wound. The combination therapy of hydrogel and hUC-MSCs sped up wound closure. The combination therapy of hydrogel and hUC-MSCs upregulated the relative gene expressions of EGF, TGF-β1, VEGF, and VEGFA, which promoting epithelial regeneration and angiogenesis.

Conclusions: The fibrin hydrogel scaffold provides a relatively stable sterile environment for cell adhesion, proliferation, and migration and prolongs cell survival at the wound site. The hydrogel-hUC-MSC combination therapy can promote wound closure, re-epithelialization, and neovascularization. It exhibits a remarkable therapeutic effect than hUC-MSCs or the hydrogel alone.

1 Background

As the largest organ of the human body, the skin is the first barrier against the external environment, preventing external damage and microbial invasion and maintaining the normal physiological environment [1–3]. Once the skin is damaged, the wound will disable the barrier function and even threaten people's lives in severe cases. Full-thickness skin wound can result from all kinds of injuries, such as acute trauma, chronic ulcers, and deep burns, and can cause many physiological and functional problems [4].

In recent years, the advantages of mesenchymal stem cell (MSC) transplantation for skin wound healing has attracted extensive attention in skin-related research. Researchers have proved that MSCs play important roles in all stages of wound healing [5–9]. However, further studies are necessary to solve problems, such as collection, short survival time, and immunological rejection.

MSCs can be obtained from various sources, including the bone marrow, adipose tissue, umbilical cord, Wharton's jelly, and placenta [10]. Among them, human umbilical cord MSCs (hUC-MSCs) have the advantages of painless collection, no ethical dispute, fast self-renewal, low immunogenicity, and more clinical application prospects than other MSCs [11–13]. Studies have shown that hUC-MSCs can accelerate wound healing, inhibit the inflammatory response, promote re-epithelialization, and increase angiogenesis without serious complications or adverse reactions [14–19].

At present, traditional cotton medical gauze is widely used as the clinical routine dressing, but it has some inevitable disadvantages, such as limited use, difficulty in absorption, and frequent replacement, which may cause secondary trauma. Biological dressings, including pig skin and amniotic membrane, carry the risk of spreading bacteria and viruses and immunological rejection [20–23]. Alternatively, hydrogels are considered a more ideal wound treatment material. Hydrogels have good biocompatibility, can prevent the loss of water and body fluid from wounds, and their biodegradability can avoid secondary damage during dressing change. They are easy to use, especially suitable for irregular wounds, and can resist bacterial invasion [24–26]. Moreover, the three-dimensional mesh structure and low cytotoxicity of hydrogels provide a suitable environment for cell adhesion and proliferation, prolong the survival of cells around the wound, and have a broad application prospect in tissue engineering and drug-controlled release fields [27–30].

Herein, we developed a fibrin hydrogel scaffold, formed by the interaction of fibrinogen and thrombin. With its excellent biocompatibility and safety, the fibrin hydrogel is authorized by the Food and Drug Administration for use in the human body [31–33]. In this study, we engineered a fibrin hydrogel scaffold loaded with hUC-MSCs to be implanted into the wound area for the treatment of full-thickness skin defects in a mouse model, aiming to explore the wound healing effects of fibrin hydrogel scaffold loaded with hUC-MSCs.

2 Materials And Methods

2.1 Synthesis of the fibrin hydrogel scaffold

Freeze-dried fibrinogen powder (F8051, Solarbio, China) was dissolved in sterilized water to make up 10 mg/mL fibrinogen solution. Freeze-dried thrombin powder (T8021, Solarbio, China) was dissolved in calcium ion solution (containing 300 mmol/L sodium chloride, 40 mmol/L calcium chloride) to make up 25 U/mL thrombin solution. Fibrinogen and thrombin solutions were mixed at a ratio of 1:1 (v/v) to synthesize fibrin hydrogel scaffolds.

2.2 Characterization of the fibrin hydrogel scaffold

2.2.1 Field emission scanning electron microscopy (FESEM) characterization

Fibrin hydrogel scaffolds were characterized using FESEM (S4800, Hitachi, Japan). The fibrin hydrogel was shaped into a lyophilized scaffold using a vacuum freeze dryer (LICHEN LC-10N-50C), fixed on a copper bar, and sprayed with gold. Then, the morphology of the hydrogel scaffold was observed via FESEM.

2.2.2 In vitro degradation of the fibrin hydrogel scaffold

Fibrin hydrogel scaffolds were immersed in phosphate-buffered saline (PBS) and placed in a biosafety cabinet. Scaffolds were taken out at intervals to drain off surface moisture, and the remaining mass was weighed. Then, the degradation rate was calculated using the following formula:

Degradation rate (%) = (Wi - Wr)/Wi × 100%,

where Wi is the Initial weight of the hydrogel, and Wr is the remaining weight of the hydrogel.

2.3 Fibrin hydrogel scaffold toxicity analysis

The cytotoxicity of the fibrin hydrogel was determined via cell counting kit-8 (CCK-8) assay. Hydrogels were pretreated with culture media in an incubator at 37 °C, 5% CO_2 for 24 h. The supernatant was collected and filter sterilized as the 100% hydrogel extract. The extract was then used to culture hUC-MSCs for 24 or 48 h. Subsequently, 10 μL CCK-8 solution (Dojindo, Japan) was added to each well of a 96-well culture plate, and the plate was incubated for 4 h in the incubator. Finally, the absorbance at 450 nm was measured immediately using a microplate reader.

2.4 Isolation and culture of hUC-MSCs

Human umbilical cord tissues were obtained from a cesarean section at the Obstetrics and Gynecology Department of the First Affiliated Hospital of Soochow University. Informed consent was obtained from patients. The human umbilical cord tissue sampling schemes were approved by the Ethics Review Committee of the First Affiliated Hospital of Soochow University. Briefly, several segments of the fresh umbilical cord tissue (3 cm each) were collected under aseptic conditions in the operating room, rinsed several times with sterile saline to remove blood clots, placed in sterile boxes containing PBS, supplemented with 100 U/mL penicillin and 100 μg/mL streptomycin on ice, and transported to the laboratory immediately. The umbilical cords were washed several times again with PBS supplemented with 100 U/mL penicillin and 100 μg/mL streptomycin and cut into 1 mm^3 fragments with a surgical scissor. The fragments were placed in a Petri dish and a small amount of DMEM/F12 (C11330500BT, Gibco, USA) with 10% FBS (10099-141, Gibco, USA) was added. The dish was incubated in an incubator at 37 °C and 5% CO_2, and the medium was added regularly. The fragments were removed when a large number of cells migrated out. The cells were passaged when they reached 80% confluence. HUC-MSCs at passages 2–5 were used for the following experiments.

2.5 Flow cytometry

HUC-MSCs surface antigens were detected using flow cytometer between the second and the fifth passages. In total, 1×10^6 suspended cells were incubated with 0.5% bovine serum albumin (BSA)/PBS at 4 °C for 30 min to block non-specific antigens. The cells were then incubated lucifugally with fluorescein isothiocyanate (FITC)-labeled anti-mouse CD45 (Biolegend) and CD90 (Biolegend), as well as phycoerythrin (PE)-labeled anti-mouse CD34 (Biolegend) and CD105 (Biolegend), at 4 °C for 60 min. Then, the cells were washed twice with 0.5% BSA/PBS and resuspended in 200 μL 0.5% BSA/PBS and analyzed using a flow cytometer (BD, LSRFortessa).

2.6 Adipogenic and osteoblastic differentiation of hUC-MSCs

Adipogenic and osteoblastic differentiation assays were performed to detect the multidirectional differentiation potential of the hUC-MSCs. Adipogenic differentiation was induced using the adipogenic induction medium (Stemcell, Canada). The medium was changed every 3 days and oil red O staining was performed on day 14. Osteogenic differentiation was induced using the osteogenic induction medium (Cyagen, USA). The medium was changed every 3 days, and alizarin red staining was performed on day 21.

2.7 Wound model

All animals were treated following the National Institutes of Health Guide for the Care and Use of Laboratory Animals. The protocol was approved by the Ethics Review Committee of the First Affiliated Hospital of Soochow University. Briefly, 36 female specific-pathogen-free-class BALB/c mice aged 8 weeks were randomly divided into four groups: control group (n = 9); hydrogel-alone group (n = 9); hUC-MSC-alone group (n = 9); and hydrogel-hUC-MSC combination group (n = 9). The mice were anesthetized using an initial high concentration (2% isoflurane, 2L/min) inhalation gas via an anesthesia machine (RWD, R540, China) and maintained at a low concentration (0.5%-1% isoflurane, 1L/min). Mice were placed on a heating pad to keep them warm during the surgery. After the hairs on the back of each mouse were shaved with a shaver, the remaining hairs were removed with depilatory cream. Then, entoiodine was applied three times to disinfect the back skin. Next, full-thickness skin wounds with a diameter of 8 mm were established at the midline of the back of each mouse using a skin perforator. Then, PBS, fibrin hydrogel, hUC-MSCs or fibrin hydrogel loaded with hUC-MSCs were injected into wounds, respectively. All wounds were covered with antibacterial film (Drape Antimicrob 35 × 35CM BX10 6640EZ, 3M, USA) to avoid the dislocation of scaffolds and exogenous infection. There were three mice for each time point in each group, and a total of six wounds for each time point. A second dose was administered on day 7. Mice were kept in separate cages with food and water and observed daily throughout the experiment. On days 0, 3, 7, 10, and 14 after the surgery, the wound of each mice was recorded with a digital camera. The wound healing rate was calculated using the following formula:

wound healing rate (%) = (Ao - Au)/Ao × 100%,

where Ao is the original wound area, and Au is the unhealed wound area.

2.8 Histological analysis

On days 3, 7, and 14 after the surgery, the wound and surrounding tissues (diameter = 1 cm) were excised and fixed in 4% paraformaldehyde for 24 h. Samples were dehydrated in a graded ethanol series (70–100%) and prepared into 6 μm-thick serial paraffin sections. According to the standard procedures, samples were exposed to either hematoxylin and eosin (H&E) or immunofluorescent staining, including green fluorescent protein (GFP) (Abcam), keratin 10 (K10) (Abcam), and keratin 14 (K14) (Abcam). Then, the ratio of wound re-epithelialization length was calculated according to H&E staining results using the following formula:

Re-epithelialization length ratio (%) = Length of epidermis extending inward/Length between the wound edges on both sides × 100%.

2.9 RT-PCR

Total RNA was extracted from the full-thickness traumatic tissue using TRIzol reagent (Invitrogen, America) according to the manufacturer's protocol. Next, the extracted total RNA was used to synthesize cDNA using the PrimeScript RT Master Mix (TaKaRa, RR036A, Japan). RT-PCR, using TB Green Premix Ex Taq (TaKaRa, RR420A, Japan), cDNA, nuclease-free water, and the primers described below, was performed using an Applied Biosystems QuantStudio 7 Flex Real-time PCR system (Applied Biosystems, USA) with the following temperature profile: 95 °C for 10 min; 40 cycles at 95 °C for 15 s and 60 °C for 30 s. Primer sequences are as follows: Mouse vascular endothelial growth factor A (VEGFA) forward 5'-GAACCAGACCTCTCACCGGAA-3', reverse 5'-GACCCAAAGTGCTCCTCGAAG-3'; mouse vascular endothelial growth factor (VEGF) forward 5'-CATCATGGTGGTGGCTGTCTG-3', reverse 5'-CACTTCCGCTTGGCTCATCA-3'; mouse epidermal growth factor (EGF) forward 5'-CATCATGGTGGTGGCTGTCTG-3', reverse 5'-CACTTCCGCTTGGCTCATCA-3'; and mouse transforming growth factor-β1 (TGF-β1) forward 5'-CCCTATATTTGGAGCCTGGA-3', reverse 5'-CTTGCGACCCACGTAGTAGA-3'.

2.10 Statistical analysis

Statistical analysis was performed using GraphPad Prism 7.0 software. All the data were presented as the mean ± standard error of the mean. All experiments were independently repeated for at least three times. Differences among the groups were assessed using one-way analysis of variance. A value of $p < 0.05$ was considered statistically significant (significance levels: *$p < 0.05$, **$p < 0.01$, and ***$p < 0.001$).

3 Results

3.1. Synthesis and characterization of the fibrin hydrogel scaffold

Fibrin hydrogel scaffolds were formed through combining fibrinogen and thrombin solutions at a ratio of 1:1 (v/v). Thrombin cut fibrinopeptide A of the α chain N-terminal region and fibrinopeptide B of β chain N-terminal region on the E domain of fibrinogen to produce fibrin monomers. Fibrin monomers were then bound via non-covalent bonds to form soluble fibrin polymers. With the participation of calcium ions, the adjacent fibrins underwent rapid covalent crosslinking, forming insoluble and stable fibrin hydrogel. The whole process was completed within a few seconds (Fig. 1A). This process simulated hemostasis in the body. The morphology of fibrin hydrogel scaffold with a porous three-dimensional mesh microstructure was demonstrated using FESEM (Fig. 1B). CCK-8 assay showed the viability of hUC-MSCs in the medium of fibrin hydrogels (Fig. 1C). Compared with the DMEM/F12 medium-containing control, the extraction medium of fibrin hydrogels did not show any obvious toxicity. The crosslinked fibrin degraded slowly into fibrin degradation products (Fig. 1D). The integrity of the fibrin hydrogel was maintained for at least 1 week, after which the hydrogel degraded gradually within 2 weeks (Fig. 1E, F). These results showed that the fibrin hydrogel scaffold had a relatively high level of biological safety, good biodegradability, and a porous three-dimensional mesh structure, which provided a suitable environment for cell adhesion and proliferation.

3.2. HUC-MSCs possess the characteristics of stem cells and multidirectional differentiation potential

According to the criteria of human MSCs defined by the International Society for Cellular Therapy [34], hUC-MSCs were detected for plastic adherence, specific surface antigen expression, and multidirectional differentiation potential. When maintained in standard culture conditions, hUC-MSCs were observed to be spindle-shaped and plastic-adherent (Fig. 2A). Oil red O staining (Fig. 2B) and alizarin red staining (Fig. 2C) showed the formation of lipid droplets and mineralized nodules, respectively, which confirmed adipogenic and osteogenic differentiation abilities of hUC-MSCs. Moreover, flow cytometry demonstrated that these cells were positive for CD90 (> 99%) (Fig. 2D) and CD105 (> 97%) (Fig. 2E), whereas negative for CD34 (> 99%) (Fig. 2F) and CD45 (> 99%) (Fig. 2G). These results showed that the hUC-MSCs possessed the basic characteristics of MSCs, including the potential of multidirectional differentiation.

3.3. Fibrin hydrogel scaffold prolongs the survival of hUC-MSCs around the wound

Immunofluorescence results showed that many GFP-labeled hUC-MSCs (GFP-hUC-MSCs) were observed in both the hUC-MSC-alone group (Fig. 3A) and hydrogel-hUC-MSC combination group (Fig. 3B) on day 3. However, GFP-hUC-MSCs were hardly observed in the hUC-MSC-alone group on day 7 (Fig. 3C), while many GFP-hUC-MSCs were still present in the hydrogel-hUC-MSC combination group (Fig. 3D). Moreover, GFP fluorescence intensity of the hydrogel-hUC-MSC ciombination group was higher than that of the hUC-MSC-alone group on days 3 and 7 (Fig. 3E). These results indicated that the fibrin hydrogel scaffold could provide a suitable microenvironment for hUC-MSCs and prolong the survival of hUC-MSCs around the wound.

3.4. Hydrogel-hUC-MSC combination therapy accelerates wound closure

All animal experiments and treatments were performed according to standard procedures (Fig. 4A). By observing the postoperative wound healing conditions, the therapeutic effects of different methods were assessed, and the wound healing rates were calculated. We found that on days 7, 10, and 14 after the treatment, wounds of mice in the hydrogel-hUC-MSC combination group healed faster than those of mice in the other three groups. Especially on day 14, the wounds of mice in the hydrogel-hUC-MSC combination group were almost completely healed, earlier than those of mice in the other three groups (Fig. 4B). Furthermore, the wound healing rate of hydrogel-hUC-MSC combination group was significantly higher than that of the other three groups from day 7 ($p < 0.001$) (Fig. 4C). On day 3, epidermal cells migrated from the edges of the wounds in the hydrogel-hUC-MSC combination group, forming obvious epithelial tongues (Fig. 4D). On day 7, epidermal cells in the hydrogel-hUC-MSC combination group continued to proliferate and migrate to the wound (Fig. 4E). On day 14, the skin morphology of the hydrogel-hUC-MSC combination group was almost the same as that of the normal skin tissue (Fig. 4F). Meanwhile, the ratios of wound re-epithelialization length of the hydrogel-hUC-MSC combination group were all higher than those of the other three groups on days 3, 7, and 14 (Fig. 4G-I). These results suggested that the combination therapy of fibrin hydrogel and hUC-MSCs could accelerate wound closure.

3.5. Hydrogel-hUC-MSC combination therapy promotes re-epithelialization

Immunofluorescence results showed that K10 (Fig. 5A, B) and K14 (Fig. 5C, D) were expressed in the inner wound of the hydrogel-hUC-MSC combination group on days 4 and 7 after surgery and extended to the center, more than that in the other three groups. On day 3, the expression level of EGF in the hydrogel-hUC-MSC combination group were higher than those in the hydrogel-alone group and control group ($p < 0.01$). Similarly, the expression level of EGF in the hUC-MSC-alone group were higher than those in the hydrogel-alone group and control group ($p < 0.05$) (Fig. 5E). The expression level of transforming growth factor β1 (TGF-β1) in the hydrogel-hUC-MSC combination group was higher than that in the other three groups ($p < 0.001$) (Fig. 5H). However, the expression levels of EGF and TGF-β1 in the hydrogel-hUC-MSC combination group were both higher than those in the other three groups ($p < 0.05$ and $p < 0.001$, respectively) (Fig. 5F, I) on day 7. Meanwhile, the expression levels of EGF and TGF-β1 in the hydrogel-hUC-MSC combination group were still higher than those in the other three groups ($p < 0.05$ and $p < 0.001$, respectively) (Fig. 5G, J) on day 14. These results indicated that the combination therapy of fibrin hydrogel and hUC-MSCs could upregulate the expression of EGF and TGF-β1 and promote re-epithelialization.

3.6. Hydrogel-hUC-MSC combination therapy promotes neovascularization

On day 3 after treatment, we hardly saw any new blood vessels in the four groups (Fig. 6A), and the expression levels of VEGF and VEGFA among the four groups had no significant difference (Fig. 6D, G). On day 7, abundant new blood vessels were found in the hUC-MSC-alone group and hydrogel-hUC-MSC combination group, more than those in the other two groups (Fig. 6B). In addition, the expression levels of VEGF and VEGFA in the hydrogel-hUC-MSC combination group were higher than those in the other three groups ($p < 0.001$ and $p < 0.001$, respectively) (Fig. 6E, H). On day 14, the numbers of blood vessels in the hUC-MSC-alone group and hydrogel-hUC-MSC combination group were more than those in the other two groups (Fig. 6C). Furthermore, the expression level of VEGF in the hydrogel-hUC-MSC combination group were higher than those in the hydrogel-alone group and control group ($p < 0.001$). Similarly, the expression level of VEGF in the hUC-MSC-alone group were higher than those in the hydrogel-alone group and control group ($p < 0.001$) (Fig. 6F). Moreover, the expression level of VEGFA in the hydrogel-hUC-MSC combination group was higher than that in the other three groups ($p < 0.001$) (Fig. 6I). These results indicated that the combination therapy of fibrin hydrogel and hUC-MSCs could upregulate the expression of VEGF and VEGFA and promote neovascularization.

4 Discussion

In this study, we demonstrated a fibrin hydrogel scaffold consisting of fibrinogen and thrombin, which had a porous, three-dimensional mesh structure and could establish perfectly fitting shapes in irregular wounds.

Full-thickness skin wounds caused by acute trauma, chronic ulcers, and deep burns have always been an intractable medical problem, which cause many physiological and functional problems [4]. Currently, the main therapeutic methods used in clinical practice are functionally limited. For instance, traditional cotton medical gauze has some inevitable disadvantages, such as limited use, difficulty in absorption, and frequent replacement, which may cause secondary trauma. Biological dressings, including pig skin and amniotic membrane, carry the risk of spreading bacteria and viruses and immunological rejection [20–23]. It has been confirmed that MSCs play important roles in all stages of wound healing [5–9], but ensuring the survival and effective functioning of MSCs at the wound site is still a difficult problem.

Our previous work demonstrated that the fibrin hydrogel scaffold possesses sustained drug release in vitro and in vivo [33]. This scaffold not only overcomes the limitations of traditional medical dressings but also provides a suitable microenvironment for hUC-MSC growth and transplantation for the treatment of skin wounds.

The advantages of hUC-MSC transplantation in skin wound healing have become popular. HUC-MSCs secrete important growth factors necessary for re-epithelialization and angiogenesis through the paracrine effect [14–19]. Herein, we found that the fibrin hydrogel scaffold enhanced the biological functions of hUC-MSCs. It facilitated the relative gene expression of growth factors (EGF, VEGF, and VEGFA) and migration-related genes (TGF-β1), which was beneficial for re-epithelialization, angiogenesis, and extracellular matrix secretion. EGF can stimulate the migration and proliferation of epidermal cells

during re-epithelialization [35]. VEGF and VEGFA are critical for angiogenesis during the formation of the granulation tissue [36]. Newly formed blood vessels can provide regenerating tissues with enough oxygen and nutrition, which are essential to complete wound healing [37]. TGF-β1 belongs to the superfamily of transforming growth factor β, which regulates cell growth and differentiation. It can stimulate fibroblasts to synthesize large amounts of collagen, providing a temporary extracellular matrix for neovascularization, as well as proliferation and migration of basal cells. In addition, TGF-β1 can promote fibroblast transformation into myofibroblasts, achieving wound closure [35]. In the present study, the expression of these cytokines was higher in the hydrogel-hUC-MSC combination therapy group. Meanwhile, the fluorescence expression of K10 and K14 was high in the combination therapy group. Keratin intermediate filaments are major protein constituents in epithelial cells that provide mechanical support and fulfill a variety of additional functions [38]. We speculated that the formation of fibrin hydrogel simulates hemostasis, providing a microenvironment similar to the extracellular matrix for hUC-MSC growth, thus, inducing the paracrine effect of hUC-MSCs and promoting cytokine secretion. With the slow degradation of the hydrogel, cytokines are released to promote extracellular matrix production and increase secretion of cytokines, improving wound healing. This is a positive feedback regulation.

Interestingly, the ratio of wound re-epithelialization length and K10 and K14 immunofluorescence results in the hydrogel-hUC-MSC combination group were substantially better than those in the hUC-MSC-alone group, but the expression levels of EGF in the hUC-MSC-alone group and hydrogel-hUC-MSC combination group had no significant difference on day 3 after surgery. We speculated that hUC-MSCs could not function well without the microenvironment provided by the hydrogel, and thus, the increased expression of EGF in the hUC-MSC-alone group was not enough to recruit sufficient epidermal cells at the wound site. From this point of view, the positive effects of hydrogel on cell adhesion, proliferation, and migration were also supported. In addition, the expression of VEGFA in the hUC-MSC-alone group was lower than that in the hydrogel-hUC-MSC combination group, while the expression of VEGF in the hUC-MSC-alone group was similar to that in the hydrogel-hUC-MSC combination group on day 14 after surgery. We hypothesized that this might be because VEGFA is only one of the members of the VEGF family, and at this point, wound repair had already been in the late remodeling stage.

These findings strongly support the clinical therapeutic potential of the fibrin hydrogel scaffold loaded with hUC-MSCs. However, this study is not without limitations; the underlying mechanism of how fibrin hydrogel-hUC-MSC combination therapy promotes wound healing has not been discussed in our work, which needs further investigation.

5 Conclusion

To conclude, we have demonstrated the therapeutic effect of fibrin hydrogel scaffold loaded with hUC-MSCs on full-thickness skin defect healing. The fibrin hydrogel scaffold can adapt to a variety of irregularly shaped skin wounds. It provides a relatively stable sterile environment for cell adhesion, proliferation, and migration and prolongs cell survival at the wound site. The hydrogel-hUC-MSC combination therapy has positive effects on the wound closure, re-epithelialization, and

neovascularization. It exhibits a remarkable therapeutic effect than hUC-MSCs or the hydrogel alone. Our study provides a promising strategy and support for the clinical treatment of skin wound healing.

6 Abbreviations

MSC: Mesenchymal stem cell; hUC-MSCs: human umbilical cord mesenchymal stem cells; FESEM: Field emission scanning electron microscopy; PBS: Phosphate-buffered saline; CCK-8: Cell counting kit-8; BSA: Bovine serum albumin; FITC: Fluorescein isothiocyanate; PE: Phycoerythrin; H&E: Hematoxylin and eosin; GFP: Green fluorescent protein; K10: Keratin 10; K14: Keratin 14; VEGFA: Vascular endothelial growth factor A; VEGF: Vascular endothelial growth factor; EGF: Epidermal growth factor; TGF-β1: Transforming growth factor-β1; GFP-hUC-MSCs: GFP-labeled hUC-MSCs.

Declarations

Acknowledgments

Not applicable.

Author' Contributions

Lz Hu, Jh Zhou, and Zs He contributed equally to this work. S Yu, Jz Zhang, and Yg Chen designed the experiments. Lz Hu, Jh Zhou, Zs He, L Zhang, Fz Du, Mt Nie, Y Zhou, H Hao, Lx Zhang performed the experiments. Lz Hu, S Yu, Jz Zhang, Yg Chen analyzed the data, wrote the paper, and revised the manuscript. The authors read and approved the final manuscript.

Funding

This work was supported by National Natural Science Foundation of China (No. 81772773, 81400200, 81672560); the Strategic Priority Research Program of the Chinese Academy of Sciences (XDA16020807); the Key Research and Development Program of Jiangsu Province, China (BE2018668, BE2017669); Jiangsu Provincial Medical Youth Talent (QNRC2016753); the Major Innovative Research Team of Suzhou, China (ZXT2019007); Suzhou Clinical Key Technology Project (LCZX201705); Gusu Medical Youth Talent (GSWS2019034); and The Project of Jiangsu Provincial Maternal and Child Health Association (FYX201709).

Availablity of data and materials

All the data supporting the findings will be made public and can be shared by contacting the corresponding authors S Y, Jz Z, and Yg C.

Ethic approval and consent to participate

This study was approved by the Ethics Review Committee of the First Affiliated Hospital of Soochow University.

Consent for publication

Not applicable.

Competing interests

The authors declare that they have no competing interests.

References

1. Zheng Z, Bian S, Li Z, Zhang Z, Liu Y, Zhai X, et al. Catechol modified quaternized chitosan enhanced wet adhesive and antibacterial properties of injectable thermo-sensitive hydrogel for wound healing. Carbohydr Polym 2020, 249:116826.
2. Lei Z, Singh G, Min Z, Shixuan C, Xu K, Pengcheng X, et al. Bone marrow-derived mesenchymal stem cells laden novel thermo-sensitive hydrogel for the management of severe skin wound healing. Mater Sci Eng C Mater Biol Appl 2018, 90:159-167.
3. Sadiq A, Shah A, Jeschke MG, Belo C, Qasim Hayat M, Murad S, et al. The Role of Serotonin during Skin Healing in Post-Thermal Injury. Int J Mol Sci 2018, 19(4).
4. Gurtner G, Werner S, Barrandon Y, Longaker M. Wound repair and regeneration. Nature 2008, 453(7193):314-321.
5. Walter MNM, Wright KT, Fuller HR, MacNeil S, Johnson WEB. Mesenchymal stem cell-conditioned medium accelerates skin wound healing: An in vitro study of fibroblast and keratinocyte scratch assays. Exp Cell Res 2010, 316(7).
6. Jeon YK, Jang YH, Yoo DR, Kim SN, Lee SK, Nam MJ. Mesenchymal stem cells' interaction with skin: wound-healing effect on fibroblast cells and skin tissue. Wound Repair Regen 2010, 18(6):655-661.
7. MD GL, PhD, MD WC, PhD WH, MD XW, PhD, MD JT, MD MF, et al. Promotion of cutaneous wound healing by local application of mesenchymal stem cells derived from human umbilical cord blood. Wound Repair Regen 2010, 18(5).
8. Schlosser S, Dennler C, Schweizer R, Eberli D, Stein JV, Enzmann V, et al. Paracrine effects of mesenchymal stem cells enhance vascular regeneration in ischemic murine skin. Microvascular Research 2012, 83(3).
9. Jianying G, Ninghua L, Xinrong Y, Zihao F, Fazhi Q. Adiposed-derived stem cells seeded on PLCL/P123 eletrospun nanofibrous scaffold enhance wound healing. Biomedical materials (Bristol, England) 2014, 9(3).
10. Lee DE, Ayoub N, Agrawal DK. Mesenchymal stem cells and cutaneous wound healing: novel methods to increase cell delivery and therapeutic efficacy. Stem Cell Res Ther 2016, 7:37.

11. Ding DC, Chang YH, Shyu WC, Lin SZ. Human umbilical cord mesenchymal stem cells: a new era for stem cell therapy. Cell Transplant 2015, 24(3):339-347.
12. Shi Y, Wang Y, Li Q, Liu K, Hou J, Shao C, et al. Immunoregulatory mechanisms of mesenchymal stem and stromal cells in inflammatory diseases. Nat Rev Nephrol 2018, 14(8):493-507.
13. Li S, Wang Y, Guan L, Ji M. Characteristics of human umbilical cord mesenchymal stem cells during ex vivo expansion. Mol Med Rep 2015, 12(3):4320-4325.
14. S DM. Human umbilical cord mesenchymal stromal cells in regenerative medicine. Stem cell research & therapy 2013, 4(6).
15. Qin H, Zhu X, Zhang B, Zhou L, Wang W. Clinical Evaluation of Human Umbilical Cord Mesenchymal Stem Cell Transplantation After Angioplasty for Diabetic Foot. Exp Clin Endocrinol Diabetes 2016.
16. Yang J, Chen Z, Pan D, Li H, Shen J. Umbilical Cord-Derived Mesenchymal Stem Cell-Derived Exosomes Combined Pluronic F127 Hydrogel Promote Chronic Diabetic Wound Healing and Complete Skin Regeneration. Int J Nanomedicine 2020, 15:5911-5926.
17. Liu L, Yu Y, Hou Y, Chai J, Duan H, Chu W, et al. Human umbilical cord mesenchymal stem cells transplantation promotes cutaneous wound healing of severe burned rats. PloS one 2014, 9(2):e88348.
18. Shi H, Xu X, Zhang B, Xu J, Pan Z, Gong A, et al. 3,3'-Diindolylmethane stimulates exosomal Wnt11 autocrine signaling in human umbilical cord mesenchymal stem cells to enhance wound healing. Theranostics 2017, 7(6):1674-1688.
19. Wang S, Yang H, Tang Z, Long G, Huang W. Wound Dressing Model of Human Umbilical Cord Mesenchymal Stem Cells-Alginates Complex Promotes Skin Wound Healing by Paracrine Signaling. Stem cells international 2016, 2016:3269267.
20. S. Geetha Priya HJ, and Ashok Kumar. Skin Tissue Engineering for Tissue Repair and Regeneration. Tissue Engineering Part B: Reviews 2008, 14(1):105-118.
21. Dini V, Romanelli M, Piaggesi A, Stefani A, Mosca F. Cutaneous Tissue Engineering and Lower Extremity Wounds (Part 2). The International Journal of Lower Extremity Wounds 2006, 5(1):27-34.
22. Garlick JA. Engineering Skin to Study Human Disease – Tissue Models for Cancer Biology and Wound Repair. Advances in Biochemical Engineering/biotechnology 2007, 103:207.
23. L. M, R.A.F. C. Tissue Engineering for Cutaneous Wounds: Selecting the Proper Time and Space for Growth Factors, Cells and the Extracellular Matrix. Skin Pharmacology and Physiology 2009, 22(2).
24. Sun Y, Nan D, Jin H, Qu X. Recent advances of injectable hydrogels for drug delivery and tissue engineering applications. Polymer Testing 2020, 81.
25. Drury JL, Mooney DJ. Hydrogels for tissue engineering: scaffold design variables and applications. Biomaterials 2003, 24(24).
26. Mehrali M, Thakur A, Pennisi CP, Talebian S, Arpanaei A, Nikkhah M, et al. Nanoreinforced Hydrogels for Tissue Engineering: Biomaterials that are Compatible with Load-Bearing and Electroactive Tissues. Advanced Materials 2017, 29(8):1603612.

27. Sivashanmugam A, Arun Kumar R, Vishnu Priya M, Nair SV, Jayakumar R. An overview of injectable polymeric hydrogels for tissue engineering. European Polymer Journal 2015, 72:543-565.
28. Alexander A, Ajazuddin, Khan J, Saraf S, Saraf S. Poly(ethylene glycol)-poly(lactic-co-glycolic acid) based thermosensitive injectable hydrogels for biomedical applications. J Control Release 2013, 172(3):715-729.
29. Kopecek J. Hydrogel biomaterials: a smart future? Biomaterials 2007, 28(34):5185-5192.
30. Tsou YH, Khoneisser J, Huang PC, Xu X. Hydrogel as a bioactive material to regulate stem cell fate. Bioact Mater 2016, 1(1):39-55.
31. Chen Q, Wang C, Zhang X, Chen G, Hu Q, Li H, et al. In situ sprayed bioresponsive immunotherapeutic gel for post-surgical cancer treatment. Nat Nanotechnol 2019, 14(1):89-97.
32. Losi P, Briganti E, Errico C, Lisella A, Sanguinetti E, Chiellini F, et al. Fibrin-based scaffold incorporating VEGF- and bFGF-loaded nanoparticles stimulates wound healing in diabetic mice. Acta biomaterialia 2013, 9(8):7814-7821.
33. Zhang L, Zhou J, Hu L, Han X, Zou X, Chen Q, et al. In Situ Formed Fibrin Scaffold with Cyclophosphamide to Synergize with Immune Checkpoint Blockade for Inhibition of Cancer Recurrence after Surgery. Advanced Functional Materials 2019, 30(7).
34. Dominici M, Le Blanc K, Mueller I, Slaper-Cortenbach I, Marini F, Krause D, et al. Minimal criteria for defining multipotent mesenchymal stromal cells. The International Society for Cellular Therapy position statement. Cytotherapy 2006, 8(4):315-317.
35. Singer A, Clark R. Cutaneous wound healing. The New England journal of medicine 1999, 341(10):738-746.
36. Nissen N, Polverini P, Koch A, Volin M, Gamelli R, DiPietro L. Vascular endothelial growth factor mediates angiogenic activity during the proliferative phase of wound healing. The American journal of pathology 1998, 152(6):1445-1452.
37. Chen S, Wang H, Su Y, John JV, McCarthy A, Wong SL, et al. Mesenchymal stem cell-laden, personalized 3D scaffolds with controlled structure and fiber alignment promote diabetic wound healing. Acta Biomater 2020, 108:153-167.
38. Schweizer J, Bowden PE, Coulombe PA, Langbein L, Lane EB, Magin TM, et al. New consensus nomenclature for mammalian keratins. J Cell Biol 2006, 174(2):169-174.

Figures

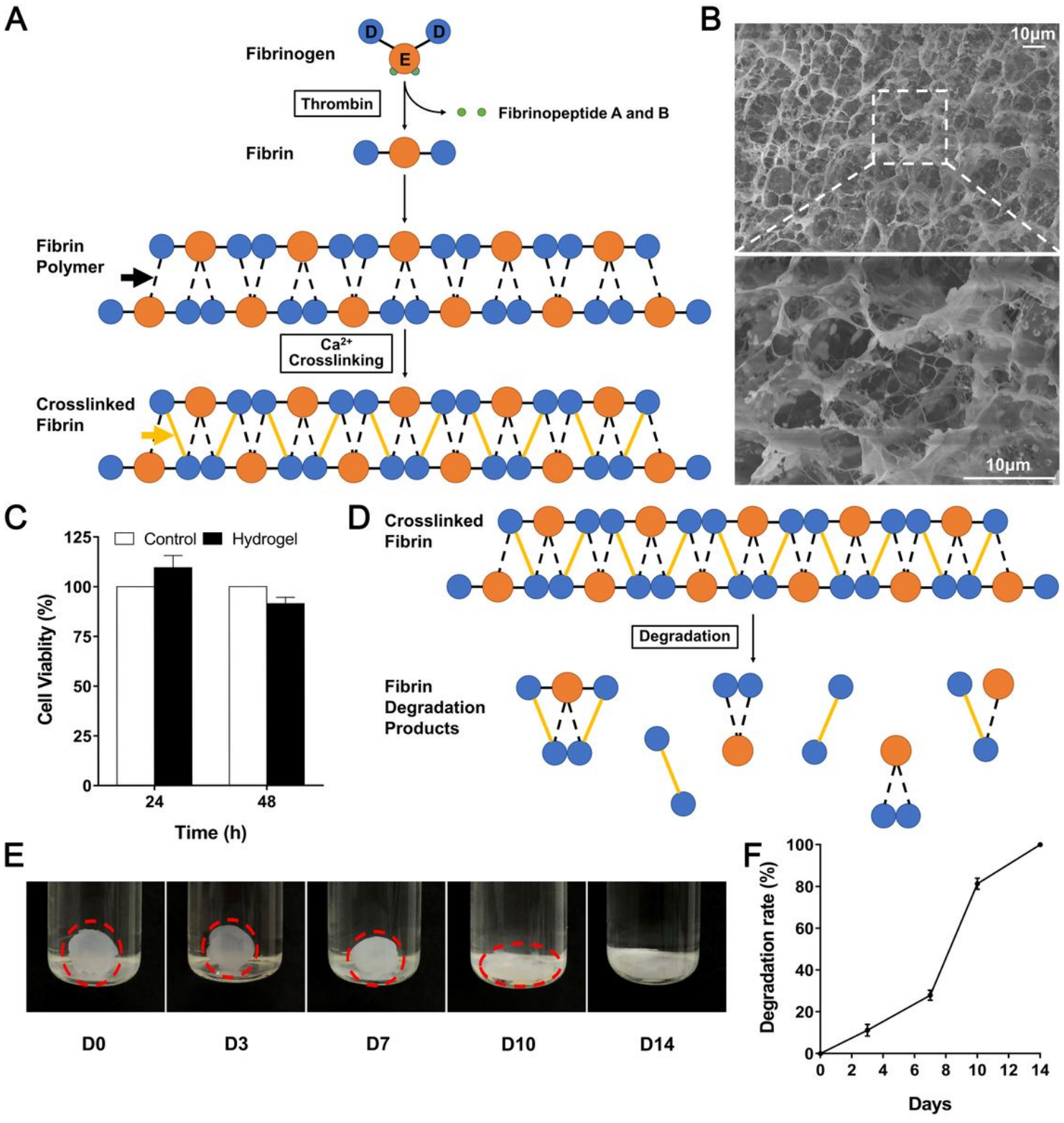

Figure 1

Synthesis and characterization of fibrin hydrogel scaffold. A) Schematic diagram of fibrinogen and thrombin combing to form the fibrin hydrogel. B) Representative image of FESEM image of fibrin hydrogel. C) Cytotoxicity of hydrogel against to hUC-MSCs incubated in DMEM/F12 at 24h and 48h. D) Schematic diagram of hydrogel degradation. E) In vitro degradation behavior and F) degradation rate of

hydrogel in PBS buffer over 14 days. Black arrow: non-covalent bond. Yellow arrow: covalent bond. Scale bar = 10μm. Data were presented by mean ± SEM.

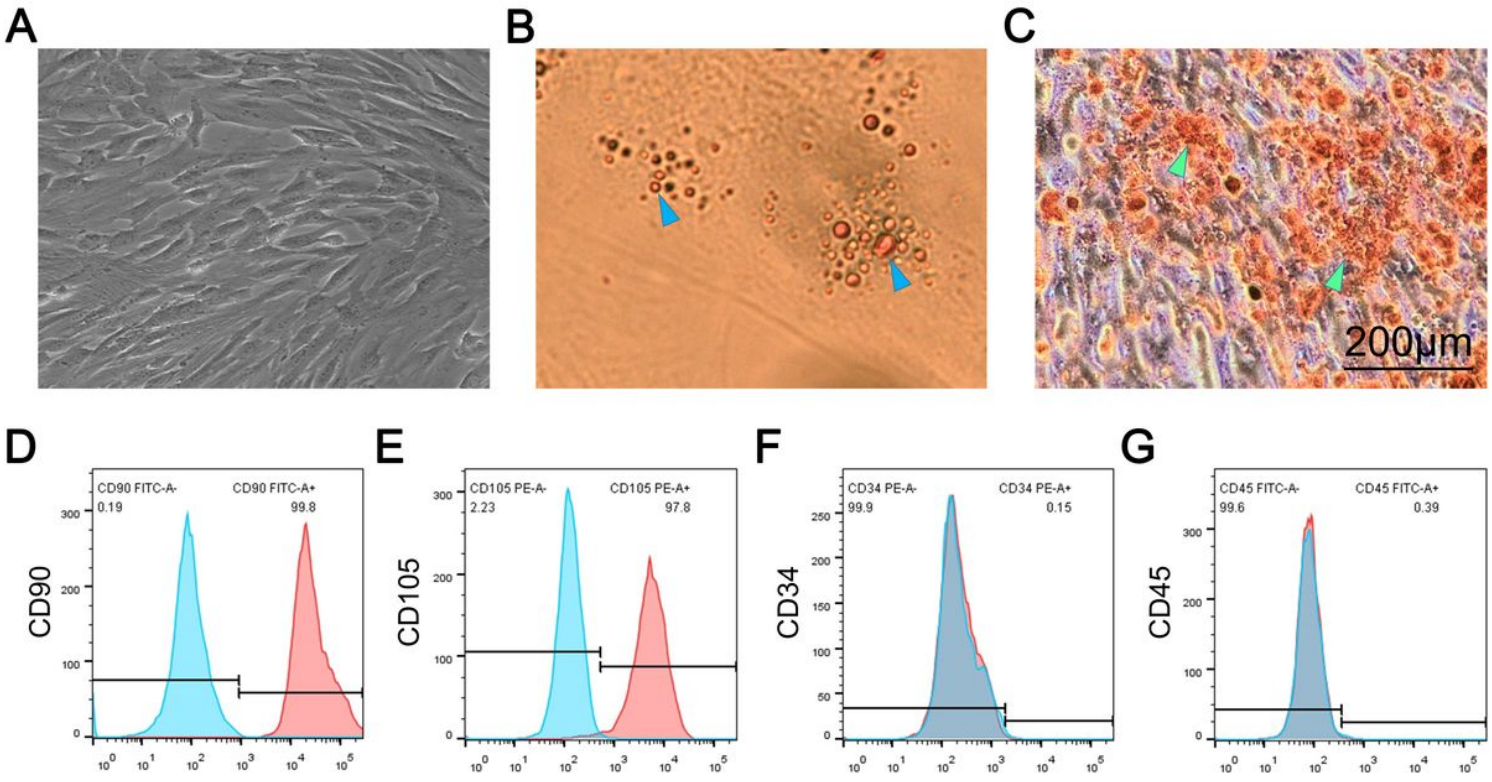

Figure 2

HUC-MSCs possess the characteristics of stem cells and multidirectional differentiation potential. A) Microscopic morphology of hUC-MSCs. B) Oil red O staining showed lipid droplets (blue arrowheads) formation. C) Alizarin red staining showed mineralized nodules (green arrowheads) formation. D-G) Flow cytometric analysis of surface antigens in hUC-MSCs. Scale bar = 200μm.

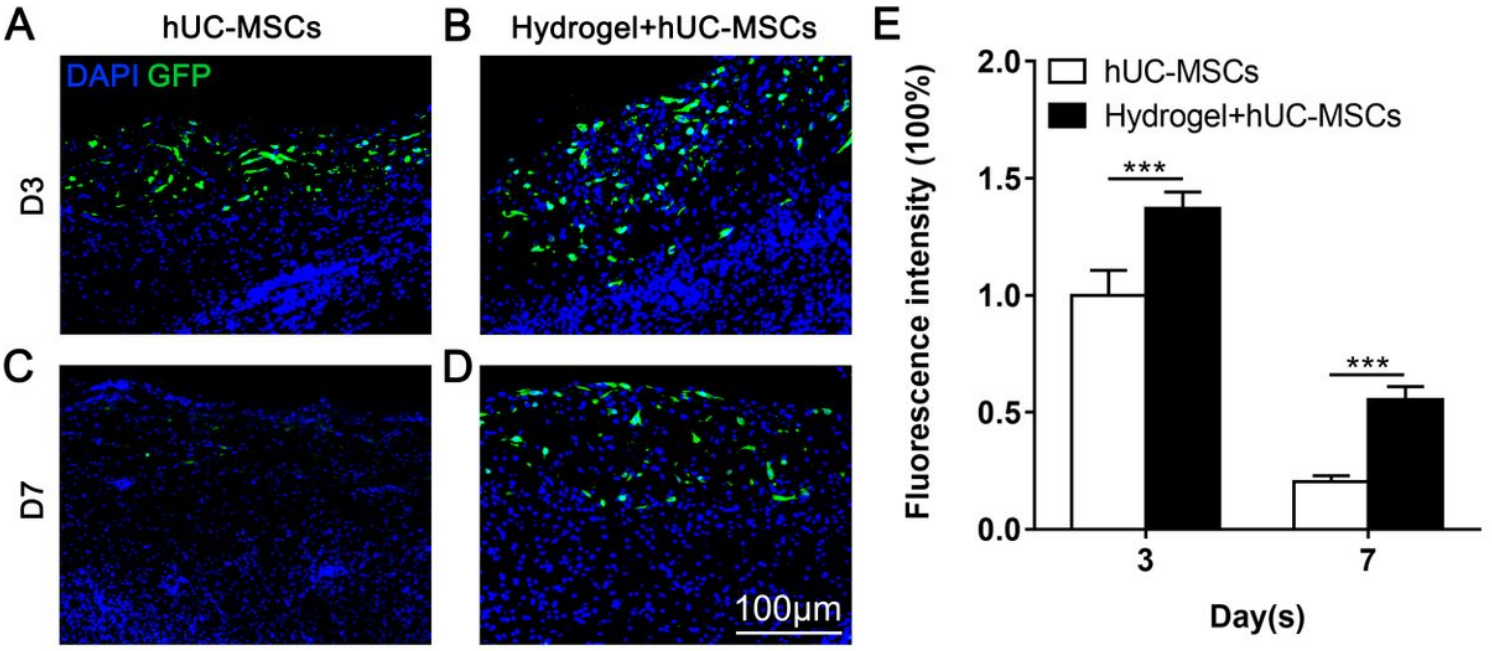

Figure 3

Fibrin hydrogel scaffold prolongs the survival time of hUC-MSCs at the wound site. Skin wounds were transplanted with GFP-labelled hUC-MSCs or hydrogel-GFP-labelled hUC-MSCs. A, B) Fluorescence tracer results in vivo on day 3 after surgery. C, D) Fluorescence tracer results in vivo on day 7 after surgery. E) Comparison of GFP fluorescence intensity between the hUC-MSCs-alone group and hydrogel-hUC-MSCs combination group on day 3 and 7 after surgery. Scale bar = 100μm. Data were presented by mean ± SEM. ***p < 0.001.

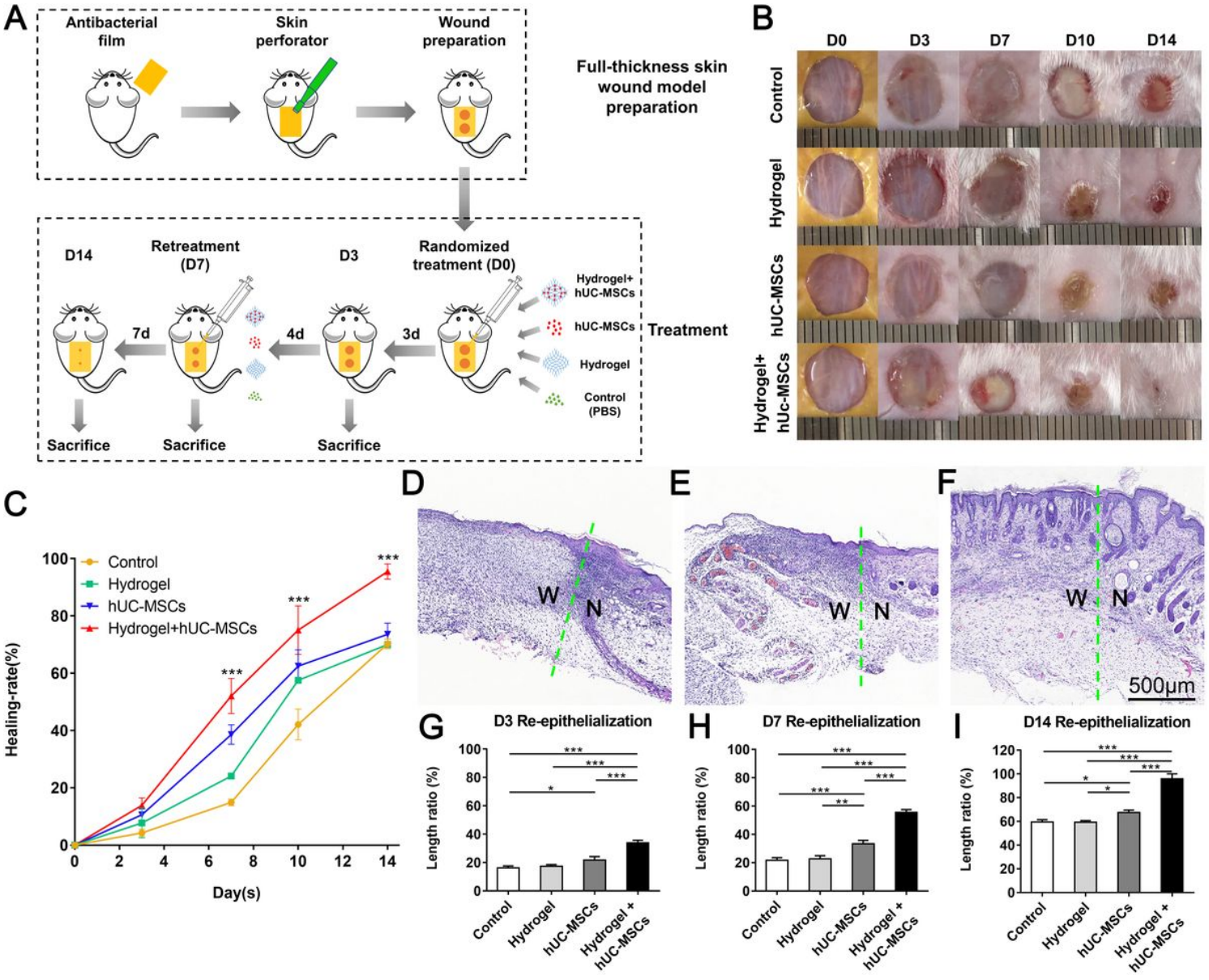

Figure 4

Hydrogel-hUC-MSCs combination therapy promotes wound closure. A) The flow diagram of animal modeling and treatment. B) Wound healing conditions of the mice in the control group, hydrogel-alone group, hUC-MSCs-alone group and hydrogel-hUC-MSCs combination group on day 3, day 7, day 10 and day 14 after surgery. C) Comparison of wound healing rates among the control group, hydrogel-alone group, hUC-MSCs-alone group and hydrogel-hUC-MSCs combination group on day 3, day 7, day 10 and day 14 after surgery. D) H&E staining of the wound in the hydrogel-hUC-MSCs combination group on day

3 after surgery. E) H&E staining of the wound in the hydrogel-hUC-MSCs combination group on day 7 after surgery. F) H&E staining of the wound in the hydrogel-hUC-MSCs combination group on day 14 after surgery. G-I) The ratio of wound re-epithelialization length of the control group, hydrogel-alone group, hUC-MSCs-alone group and hydrogel-hUC-MSCs combination group on day 3, day 7 and day 14 after surgery. Green dotted line shows the edge of the wound, W: wound area, N: normal area. Scale bar = 500μm. Data were presented by mean ± SEM. *p < 0.05, **p < 0.01 and ***p < 0.001.

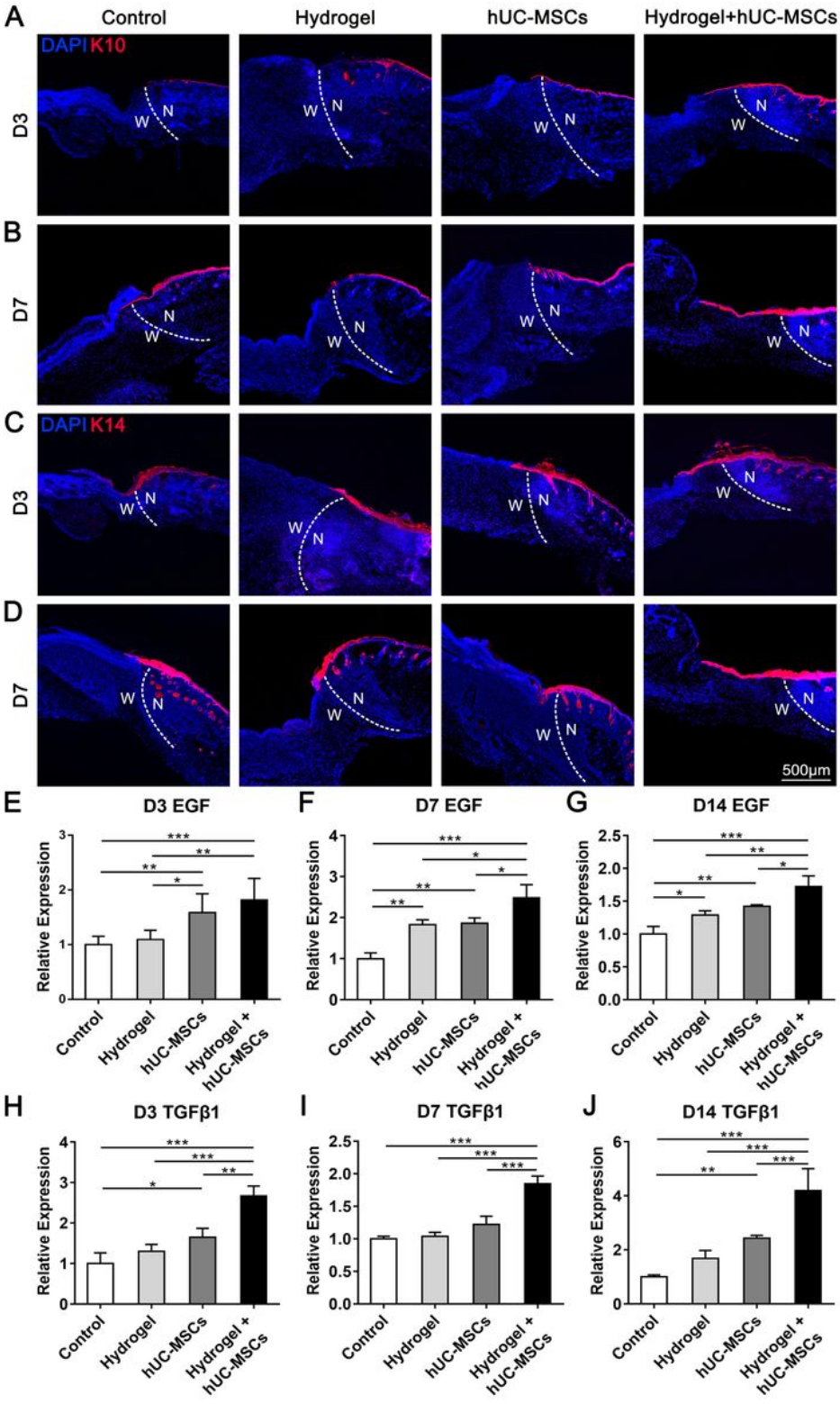

Figure 5

Hydrogel-hUC-MSCs combination therapy promotes re-epithelialization. A, B) Keratin 10 immunofluorescence results of the wounds in the control group, hydrogel-alone group, hUC-MSCs-alone group and hydrogel-hUC-MSCs combination group on day 3 and day 7 after surgery. C, D) Keratin 14 immunofluorescence results of the wounds in the control group, hydrogel-alone group, hUC-MSCs-alone group and hydrogel-hUC-MSCs combination group on day 3 and day 7 after surgery. E-G) Expression levels of EGF in the control group, hydrogel-alone group, hUC-MSCs-alone group and hydrogel-hUC-MSCs combination group on day 3, day 7 and day 14 after surgery. H-J) Expression levels of TGF-β1 in the control group, hydrogel-alone group, hUC-MSCs-alone group and hydrogel-hUC-MSCs combination group on day 3, day 7 and day 14 after surgery. White dotted line shows the edge of the wound, W: wound area, N: normal area. Scale bar = 500μm. Data were presented by mean ± SEM. *$p < 0.05$, **$p < 0.01$ and ***$p < 0.001$.

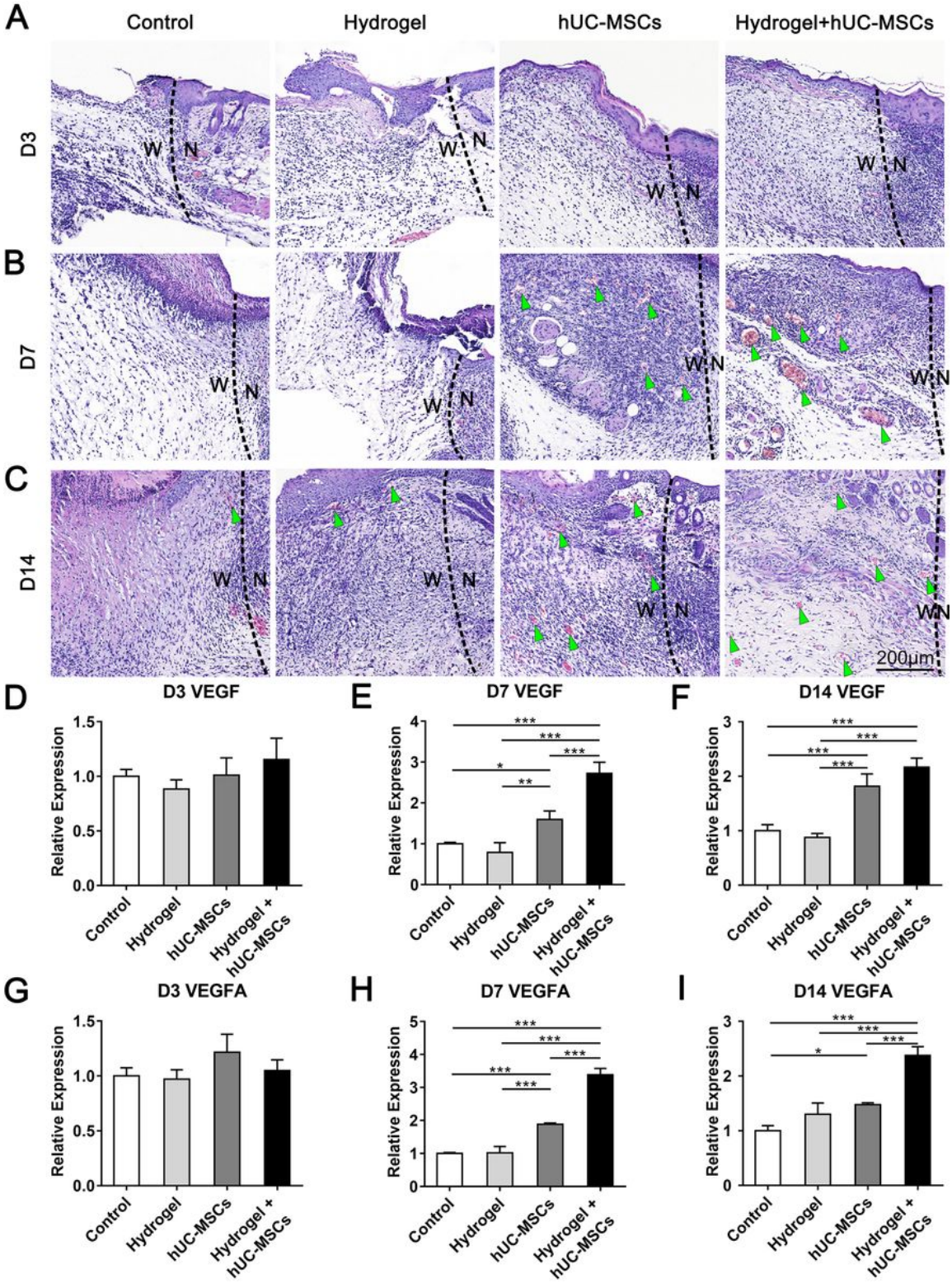

Figure 6

Hydrogel-hUC-MSCs combination therapy promotes neovascularization. A-C) H&E staining of the wounds in the control group, hydrogel-alone group, hUC-MSCs-alone group and hydrogel-hUC-MSCs combination group on day 3, day 7 and day 14 after surgery. D-F) Expression levels of VEGF in the control group, hydrogel-alone group, hUC-MSCs-alone group and hydrogel-hUC-MSCs combination group on day 3, day 7 and day 14 after surgery. G-I) Expression levels of VEGFA in the control group, hydrogel-alone group,

hUC-MSCs-alone group and hydrogel-hUC-MSCs combination group on day 3, day 7 and day 14 after surgery. Black dotted line shows the edge of the wound. Green arrowhead: Blood vessel. W: wound area, N: normal area. Scale bar = 200μm. Data were presented by mean ± SEM. *p < 0.05, **p < 0.01 and ***p < 0.001.